A numerical study of forced magnetic reconnection in the viscous Taylor problem

Richard Fitzpatrick[a)]
Center for Magnetic Reconnection Studies, Institute for Fusion Studies, Department of Physics, University of Texas at Austin, Austin, Texas 78712

(Received 22 November 2002; accepted 21 March 2003)

Two-dimensional, nonlinear magnetohydrodynamical simulations are used to investigate the so-called Taylor problem, in which a small amplitude boundary perturbation is suddenly applied to a tearing stable, slab plasma equilibrium—the perturbation being such as to drive magnetic reconnection within the plasma. This type of reconnection, which is not due to an intrinsic plasma instability, is generally known as ''forced reconnection.'' For numerical reasons, the investigation is restricted to the large magnetic Prandtl number limit. The simulation results are highly consistent with the analysis of Hahm and Kulsrud [Phys. Fluids **28**, 2412 (1985)] (modified by strong plasma viscosity). At high perturbation amplitudes, the system exhibits a phase of Sweet–Parker reconnection, as predicted by Wang and Bhattacharjee [Phys. Fluids B **4**, 1795 (1992)]. An expression for the threshold perturbation amplitude required to trigger Sweet–Parker reconnection is derived, and successfully benchmarked against numerical simulations. This expression suggests that a Sweet–Parker phase is only likely to occur during forced reconnection in tokamaks when the plasma is extremely hot and perturbation amplitude relatively large. © *2003 American Institute of Physics.* [DOI: 10.1063/1.1574516]

I. INTRODUCTION

In this paper a model resistive MHD (magnetohydrodynamical) problem which was first proposed by J. B. Taylor was investigated. In this problem, a stable slab equilibrium is subject to a suddenly imposed, small amplitude boundary perturbation which is such as to drive magnetic reconnection, and associated island chain formation, at the center of the slab. This type of reconnection, which is not due to an intrinsic plasma instability, is generally termed ''forced reconnection.'' The aim of the investigation is to describe the sequence of events from the imposition of the boundary perturbation to the establishment of the island chain within the plasma.

The so-called ''Taylor problem'' is of great intrinsic interest to plasma physicists,[1–9] but also has practical applications. Within the context of tokamak experiments, it is often the case that magnetic reconnection is driven in otherwise tearing stable plasmas by so-called ''error-fields,'' which are small nonaxisymmetric magnetic perturbations generated by field-coil misalignments.[10,11] It is also possible for MHD instabilities, such as sawtooth crashes and ELMs (edge localized modes), to generate magnetic perturbations which drive reconnection elsewhere within the plasma.[12]

The Taylor problem was first investigated by Hahm and Kulsrud,[1] who identified five dynamical phases in the reconnection process, which they labeled A, B, C, D, and E. Phases A through D are governed by linear layer physics, whereas phase E (which was described but not explicitly assigned a label by Hahm and Kulsrud) corresponds to the well-known nonlinear magnetic island dynamics of Rutherford.[13] The Hahm and Kulsrud analysis was subsequently corrected by Wang and Bhattacharjee,[2] who pointed out that under certain circumstances the linear phase D must be replaced by a nonlinear phase W, corresponding to Sweet–Parker reconnection.[14,15]

In this paper we investigate the Taylor problem primarily via two-dimensional, nonlinear MHD simulations. For numerical reasons the investigation is restricted to the large magnetic Prandtl number limit, $\mu/\eta \gg 1$. We have two main goals. First, we hope to verify the analysis of Hahm and Kulsrud. Second, we wish to determine the criteria for the existence of a Sweet–Parker reconnection phase.

Section II outlines the basic system of equations used in our simulations. A brief survey of the relevant analytic theory is given in Sec. III. The numerical simulations themselves are presented in Sec. IV. Finally, the paper is summarized and conclusions are drawn in Sec. V.

II. PRELIMINARY ANALYSIS

A. Basic equations

Standard right-handed Cartesian coordinates (x,y,z) are adopted. It is assumed that there is no variation along the z-axis: i.e., $\partial/\partial z \equiv 0$. Consider a compressible plasma governed by equations of resistive, viscous, MHD. Let the plasma density, ρ, and viscosity, μ, both be uniform, and let the resistivity, η, be a function of x only. It follows that

$$\mathbf{B} = \nabla \wedge \mathbf{A}, \tag{1}$$

$$\mu_0 \mathbf{j} = \nabla \wedge \mathbf{B}, \tag{2}$$

$$-\frac{\partial \mathbf{A}}{\partial t} - \nabla \varphi + \mathbf{V} \wedge \mathbf{B} = \eta \mathbf{j} - \mathbf{E}_0, \tag{3}$$

a)Electronic mail: rfitzp@farside.ph.utexas.edu

$$\rho\left[\frac{\partial \mathbf{V}}{\partial t}+(\mathbf{V}\cdot\boldsymbol{\nabla})\mathbf{V}\right]=-\boldsymbol{\nabla}p+\mathbf{j}\wedge\mathbf{B}+\mu\boldsymbol{\nabla}^2\mathbf{V}, \tag{4}$$

$$\frac{\partial p}{\partial t}+\mathbf{V}\cdot\boldsymbol{\nabla}p=-\Gamma p\boldsymbol{\nabla}\cdot\mathbf{V}, \tag{5}$$

where $\mathbf{A}$ is the vector potential, φ the scalar potential, $\mathbf{B}$ the magnetic field, $\mathbf{V}$ the plasma velocity, p the plasma pressure, $\mathbf{j}$ the current density, $\mathbf{E}_0$ the (uniform) externally driven inductive electric field, and $\Gamma=5/3$ the ratio of specific heats.

Let $(x/a,y/a,z/a)\rightarrow(x,y,z)$, $t/(a/V_A)\rightarrow t$, $\mathbf{B}/B_0\rightarrow\mathbf{B}$, $\mathbf{A}/(B_0a)\rightarrow\mathbf{A}$, $\mathbf{V}/V_A\rightarrow\mathbf{V}$, $\varphi/(B_0V_Aa)\rightarrow\varphi$, $p/(\rho V_A^2)\rightarrow p$, $\mathbf{j}/(B_0/\mu_0 a)\rightarrow\mathbf{j}$, $\mathbf{E}_0/(B_0V_A)\rightarrow\mathbf{E}_0$, $\eta/\eta(0)\rightarrow\hat{\eta}$, $\eta(0)/(V_Aa\mu_0)\rightarrow\eta$, and $\mu/(V_Aa\rho)\rightarrow\mu$, where $V_A=B_0/\sqrt{\mu_0\rho}$ is the Alfvén velocity, a a convenient scale-length, and B_0 a convenient scale magnetic field-strength.

Let $\mathbf{A}(x,y,t)=[0,0,\psi(x,y,t)]$, $\mathbf{V}(x,y,t)=[u(x,y,t),v(x,y,t),0]$, $\mathbf{j}(x,y,t)=[0,0,j(x,y,t)]$, and $\mathbf{E}_0(x,y,t)=[0,0,E_0]$. It follows that

$$\frac{\partial u}{\partial t}=-u\frac{\partial u}{\partial x}-v\frac{\partial u}{\partial y}-\frac{\partial p}{\partial x}-\boldsymbol{\nabla}^2\psi\frac{\partial\psi}{\partial x}+\mu\boldsymbol{\nabla}^2u, \tag{6}$$

$$\frac{\partial v}{\partial t}=-u\frac{\partial v}{\partial x}-v\frac{\partial v}{\partial y}-\frac{\partial p}{\partial y}-\boldsymbol{\nabla}^2\psi\frac{\partial\psi}{\partial y}+\mu\boldsymbol{\nabla}^2v, \tag{7}$$

$$\frac{\partial \psi}{\partial t}=-u\frac{\partial\psi}{\partial x}-v\frac{\partial\psi}{\partial y}+\eta\hat{\eta}\boldsymbol{\nabla}^2\psi+E_0, \tag{8}$$

$$\frac{\partial p}{\partial t}=-u\frac{\partial p}{\partial x}-v\frac{\partial p}{\partial y}-\Gamma p\left(\frac{\partial u}{\partial x}+\frac{\partial v}{\partial y}\right), \tag{9}$$

where $\boldsymbol{\nabla}^2\equiv\partial^2/\partial x^2+\partial^2/\partial y^2$.

B. Plasma equilibrium

Suppose that the plasma is bounded by perfectly conducting walls located at $x=\pm X_w$, and is periodic in the y-direction with periodicity length L. The initial Harris-pinch plasma equilibrium satisfies

$$u^{(0)}(x)=0, \tag{10}$$

$$v^{(0)}(x)=0, \tag{11}$$

$$\psi^{(0)}(x)=-\ln\left(\frac{\cosh x}{\cosh X_w}\right)+\frac{x^2-X_w^2}{2\cosh^2 X_w}, \tag{12}$$

$$p^{(0)}(x)=\frac{1}{2}\left(\left[\tanh X_w-\frac{X_w}{\cosh^2 X_w}\right]^2-\left[\tanh x-\frac{x}{\cosh^2 X_w}\right]^2\right), \tag{13}$$

$$\hat{\eta}(x)=\cosh^2 x\left(\frac{\cosh^2 X_w-1}{\cosh^2 X_w-\cosh^2 x}\right). \tag{14}$$

In unnormalized units, B_0 is the equilibrium magnetic field-strength as $x\rightarrow\infty$, and a is the half-width of the current channel. Furthermore, $E_0=-\eta\hat{\eta}d^2\psi^{(0)}/dx^2$. Note the absence of equilibrium plasma flow.

C. Boundary conditions

Suppose that the conducting wall at $x=X_w$ is subject to a *small* (compared with X_w) displacement $\Xi(y,t)$ in the x-direction. An equal and opposite displacement is applied to the wall at $x=-X_w$. Of course, the displacements are periodic in y, so that $\Xi(L,t)=\Xi(0,t)$. The appropriately modified *no-slip* boundary conditions at the walls are

$$u(X_w,y,t)=-u(-X_w,y,t)=\frac{\partial\Xi(y,t)}{\partial t}, \tag{15}$$

$$v(X_w,y,t)=v(-X_w,y,t)=0, \tag{16}$$

$$\psi(X_w,y,t)=\psi(-X_w,y,t)=-\left[\frac{d\psi^{(0)}}{dx}\right]_{x=X_w}\Xi(y,t), \tag{17}$$

$$p(X_w,y,t)=p(-X_w,y,t)=-\left[\frac{dp^{(0)}}{dx}\right]_{x=X_w}\Xi(y,t). \tag{18}$$

Furthermore, all fields satisfy $A(x,L,t)=A(x,0,t)$.

III. ANALYTIC THEORY

A. Outer region

Consider the response of a tearing-stable plasma to a wall displacement of the form $\Xi(y,t)=\Xi(t)e^{-iky}$, where $k=2\pi/L$, and

$$\Xi(t)=\Xi_0(1-e^{-t/\tau_{on}}), \tag{19}$$

for $t\geqslant 0$, with $\Xi(t)=0$ for $t<0$. It is assumed that the displacement switch-on time, τ_{on}, is significantly larger than the Alfvén time, $\tau_A=a/V_A$, but much shorter than any characteristic plasma reconnection time-scale.

Conventional theory divides the plasma into an *outer* and an *inner* region, with the latter region strongly localized in the vicinity of the magnetic resonance (i.e., $x=0$). In the outer region, plasma inertia, resistivity, viscosity, and compressibility can all be neglected. In this limit, Eqs. (6)–(9) reduce to the following equation:

$$\frac{d^2\psi^{(1)}}{dx^2}-k^2\psi^{(1)}-\frac{d^3\psi^{(0)}/dx^3}{d\psi^{(0)}/dx}\psi^{(1)}=0, \tag{20}$$

where the perturbed magnetic flux is written as $\delta\psi(x,y,t)=\psi^{(1)}(x,t)e^{-iky}$. In deriving the above equation, it is assumed that the wall perturbation is relatively small (which justifies a linear approach). The boundary conditions at the conducting walls are written as

$$\psi^{(1)}(\pm X_w,t)=-\frac{d\psi^{(0)}(X_w)}{dx}\Xi(t). \tag{21}$$

Moreover, from symmetry, $\psi^{(1)}(-x,t)=\psi^{(1)}(+x,t)$. As $x\rightarrow 0$,

$$\psi^{(1)}(x,t)\rightarrow\Psi(t)+\tfrac{1}{2}\Delta\Psi(t)|x|, \tag{22}$$

where $\Psi(t)$ is the "outer" magnetic flux (which is equal to the reconnected magnetic flux in a constant-ψ response regime), and $\Delta\Psi(t)$ parametrizes the net current flowing in the inner region. It is easily demonstrated that

$$\Delta\Psi(t)=E_{ss}\Psi(t)+E_{sw}\Xi(t), \tag{23}$$

where E_{ss} and E_{sw} are real numbers obtained by solving Eq. (20) subject to the boundary conditions and symmetry constraints. Note that E_{ss} is the conventional tearing stability index (for the wave-length L tearing mode).[16] The plasma is intrinsically stable (to the wave-length L tearing mode) provided that $E_{ss}<0$, which is assumed to be the case.

B. Linear response theory

Let us first linearize Eqs. (6)–(9) and then expand about $x=0$. Next, let us Laplace transform all perturbed quantities (namely, $u^{(1)}$, $v^{(1)}$, $\psi^{(1)}$, and $p^{(1)}$): e.g.,

$$\overline{u}(x,g)=\int_0^\infty u^{(1)}(x,t)\mathrm{e}^{-gt}dt. \tag{24}$$

Finally, let us Fourier transform these quantities in the x-direction: e.g.,

$$\tilde{u}(\theta,g)=\int_{-\infty}^{\infty}\overline{u}(x,g)\mathrm{e}^{\mathrm{i}\theta kx}dx. \tag{25}$$

After some manipulation, the Fourier–Laplace transformed versions of Eqs. (6)–(9) reduce to

$$\frac{\partial}{\partial\theta}\left[\frac{\theta^2}{\alpha_g+\alpha_\eta\theta^2}\frac{\partial\tilde{\xi}}{\partial\theta}\right]-(\alpha_g+\alpha_\mu\theta^2)\theta^2\tilde{\xi}=0, \tag{26}$$

where $\tilde{\xi}(\theta,g)\propto\tilde{u}(\theta,g)/g$ is the Fourier–Laplace transformed plasma displacement in the x-direction. Furthermore, $\alpha_g=g/s$, $\alpha_\eta=k^2\eta/s$, $\alpha_\mu=k^2\mu/s$, and $s=-d^2\psi^{(0)}(0)/dx^2$. The neglect of plasma compressibility in the inner region is reasonable as long as the plasma flow velocity remains well below the sound speed, which is assumed to be the case. Now, $\tilde{\xi}(\theta,g)$ must be well-behaved as $\theta\to\infty$. Furthermore, in the limit $\theta\to0$,

$$\tilde{\xi}(\theta,g)\to\frac{\Delta(g)}{k\pi}\frac{1}{\theta}+1, \tag{27}$$

where $\Delta(g)=\overline{\Delta\Psi}(g)/\overline{\Psi}(g)$ is the layer response function.

Asymptotic matching between the inner and outer regions yields

$$\overline{\Psi}(g)=\frac{E_{sw}\overline{\Xi}(g)}{\Delta(g)-E_{ss}}, \tag{28}$$

where an overbar indicates a Laplace transformed quantity. The above expression can be inverse Laplace transformed to give the "outer" magnetic flux, $\Psi(t)$: i.e., the magnetic flux at the *edge* of the reconnecting layer. A more physically meaningful quantity is the "reconnected" magnetic flux, $\psi_0(t)\equiv\psi^{(1)}(0,t)$, which is the magnetic flux at the *center* of the reconnecting layer. The Laplace transformed reconnected flux is given by

$$\overline{\psi}_0(g)=F(g)\overline{\Psi}(g), \tag{29}$$

where

$$F(g)=-\int_0^\infty\frac{\alpha_\eta\theta^2}{\alpha_g+\alpha_\eta\theta^2}\frac{\partial\tilde{\xi}}{\partial\theta}d\theta. \tag{30}$$

Incidentally, Ishigawa and Tokuda have developed a closed formula [Eq. (25) of Ref. 7] linking the outer and reconnected magnetic fluxes in the absence of viscosity.

C. Inertial regime

In the following, we shall adopt the high viscosity ordering $\mu\gg\eta$. This ordering is relevant to tokamak experiments, and is employed in all of our numerical simulations.

Now, when $t\ll\tau_1$, where

$$\tau_1=\frac{1}{\mu^{1/3}(sk)^{2/3}}, \tag{31}$$

plasma viscosity and resistivity can be neglected in Eq. (26), which can be solved subject to the boundary condition (27) to give

$$\tilde{\xi}(\theta,g)=-\frac{\mathrm{e}^{-\alpha_g\theta}}{\alpha_g\theta}. \tag{32}$$

It follows that $\Delta=-\pi sk/g$, $F=-2\eta(sk)^2/g^3$, and

$$\overline{\psi}_0(g)=\frac{2\eta skE_{sw}\Xi_0}{\pi(1+\tau_{\mathrm{on}}g)g^3}, \tag{33}$$

where we have neglected E_{ss} with respect to Δ. The above expression can be inverse Laplace transformed to give the following expression for the reconnected flux:

$$\psi_0(t)=\psi_I(t)=E_{sw}\Xi_0\frac{\eta sk}{\pi}[t^2+2\tau_{\mathrm{on}}^2(1-\mathrm{e}^{-t/\tau_{\mathrm{on}}})-2\tau_{\mathrm{on}}t]. \tag{34}$$

The associated reconnection rate is written as

$$J_I(t)\equiv\eta^{-1}\frac{d\psi_I}{dt}=E_{sw}\Xi_0\frac{2sk}{\pi}(t+\tau_{\mathrm{on}}\mathrm{e}^{-t/\tau_{\mathrm{on}}}-\tau_{\mathrm{on}}). \tag{35}$$

D. Visco-resistive regime

Now, when $t\gg\tau_2$, where

$$\tau_2=\frac{\mu^{1/3}}{\eta^{2/3}(sk)^{2/3}}, \tag{36}$$

plasma inertia can be neglected in Eq. (26), which can be solved subject to the boundary condition (27) to give $F=1$ and

$$\Delta=\tau_{\mathrm{VR}}g, \tag{37}$$

where

$$\tau_{\mathrm{VR}}=\mathcal{A}\frac{\mu^{1/6}}{(sk)^{1/3}\eta^{5/6}}. \tag{38}$$

Here, $\mathcal{A}=\pi6^{2/3}\Gamma(5/6)/\Gamma(1/6)=2.104$. Details of the solution of Eq. (26) in this regime—which is termed the "visco-resistive" regime—are given in Ref. 17. Note that, since $F=1$ in the visco-resistive regime, there is no distinction between the outer flux and the reconnected flux—such a regime is termed a "constant-ψ" regime. (The inertial regime is characterized by $|F|\ll1$, and is, hence, a nonconstant-ψ regime.) It follows that

$$\overline{\psi_0}(g)=\frac{E_{sw}\Xi_0}{g(1+\tau_{\rm on}g)(\tau_{\rm VR}g-E_{ss})}, \tag{39}$$

which can be inverse Laplace transformed to give the following expression for the reconnected flux:

$$\psi_0(t)=\psi_{\rm VR}(t)=\frac{E_{sw}\Xi_0}{(-E_{ss})}\left[1-\frac{{\rm e}^{-t(-E_{ss})/\tau_{\rm VR}}\tau_{\rm VR}}{\tau_{\rm VR}-(-E_{ss})\tau_{\rm on}}+\frac{{\rm e}^{-t/\tau_{\rm on}}(-E_{ss})\tau_{\rm on}}{\tau_{\rm VR}-(-E_{ss})\tau_{\rm on}}\right]. \tag{40}$$

The associated reconnection rate is written as

$$J_{\rm VR}(t)\equiv\eta^{-1}\frac{d\psi_{\rm VR}}{dt}=\frac{E_{sw}\Xi_0}{\eta}\left[\frac{{\rm e}^{-t(-E_{ss})/\tau_{\rm VR}}-{\rm e}^{-t/\tau_{\rm on}}}{\tau_{\rm VR}-(-E_{ss})\tau_{\rm on}}\right]. \tag{41}$$

E. Rutherford regime

When the constant-ψ magnetic island width,

$$W(t)=4\sqrt{\frac{\psi_0(t)}{s}}, \tag{42}$$

exceeds the visco-resistive layer width,

$$\delta_{\rm VR}=4\sqrt{\mathcal{A}}\frac{(\mu\eta)^{1/6}}{(sk)^{1/3}}, \tag{43}$$

the visco-resistive regime is replaced by the Rutherford regime.[13] The Rutherford regime is a nonlinear constant-ψ regime in which the island width evolves according to the following equation:

$$\frac{\mathcal{I}}{\eta}\frac{dW(t)}{dt}=E_{ss}+\frac{E_{sw}\Xi(t)}{\psi_0(t)}. \tag{44}$$

Here, $\mathcal{I}=0.8225$. The above equation can be converted into the following expressions for the reconnected flux and reconnection rate:

$$\psi_{\rm RF}(t)=\frac{E_{sw}\Xi_0}{(-E_{ss})}y^2, \tag{45}$$

$$J_{\rm RF}(t)\equiv\eta^{-1}\frac{d\psi_{\rm RF}}{dt}=\frac{2E_{sw}\Xi_0}{\eta(-E_{ss})\tau_{\rm RF}}\left(\frac{1}{y}-y\right). \tag{46}$$

Here,

$$\tanh^{-1}y-y=\frac{t}{t_{\rm RF}}, \tag{47}$$

and

$$\tau_{\rm RF}=\frac{4\mathcal{I}}{\eta(-E_{ss})}\sqrt{\frac{E_{sw}\Xi_0}{s(-E_{ss})}}. \tag{48}$$

In deriving the above expressions, we have neglected the relatively short time-scale $\tau_{\rm on}$ with respect to the relatively long time-scale $\tau_{\rm RF}$.

F. Modified Sweet–Parker regime

Reconnection regimes are either linear or nonlinear and either constant-ψ or nonconstant-ψ. A linear regime is one in which the magnetic island width is significantly less than the linear layer width, and *vice versa* for a nonlinear regime. A constant-ψ regime is one in which the outer magnetic flux and the reconnected flux are approximately equal, and the converse for a nonconstant-ψ regime. A more physically insightful distinction between constant-ψ and nonconstant-ψ regimes is that in the former there is ample time for current to diffuse out of the reconnecting region, whereas in the latter the reconnection rate exceeds the rate of current diffusion. This distinction leads us to expect a nonconstant-ψ regime to exhibit an increasing (in time) current density in the reconnecting region, and a constant-ψ regime to exhibit a decaying current density. Let us classify the reconnection regimes we have encountered so far in this paper. The inertial regime is a linear nonconstant-ψ regime. The visco-resistive regime is a linear constant-ψ regime. Finally, the Rutherford regime is a nonlinear constant-ψ regime. We can complete our collection of reconnection regimes with a nonlinear nonconstant-ψ regime—namely, the Sweet–Parker regime.

Sweet–Parker reconnection is sufficiently well-known for us to dispense with a detailed description.[14,15] The reconnection scenario is characterized by a long narrow current sheet running along the magnetic resonance, and centered on the magnetic X-point. Magnetic flux diffuses into the sheet along its long sides and is ejected at a much higher velocity from its two ends. The presence of strong viscosity modifies the scenario somewhat from that originally described by Sweet and Parker.[18] The modified Sweet–Parker reconnection rate is given by

$$J_{\rm SP}\equiv\eta^{-1}\frac{d\psi_0}{dt}\sim\frac{\sqrt{k}(E_{sw}\Xi_0)^{3/2}}{(\mu\eta)^{1/4}}, \tag{49}$$

where we have neglected the saturation term involving E_{ss}. The $\sim$ sign in the above expression indicates that the reconnection rate is undetermined to an arbitrary [hopefully, $O(1)$] multiplicative constant. The above expression can be rearranged to give

$$\frac{J_{\rm SP}}{J_0}\sim\left(\frac{\xi_s}{\delta_{\rm VR}}\right)^{3/2}, \tag{50}$$

where $\xi_s=E_{sw}\Xi_0/s$ is the ideal-MHD plasma displacement driven at the magnetic resonance by the wall displacement. Here, $J_{\rm SP}$ is the current density within the Sweet–Parker layer (as well as a measure of the reconnection rate), whereas $J_0=s$ is the equilibrium current density at the magnetic resonance.

Forced reconnection is characterized by an initial nonconstant-ψ phase in which current density builds up in the reconnecting region, followed by a constant-ψ phase in which this current density decays away. Furthermore, the system starts off in a linear regime and subsequently makes a transition to a nonlinear regime, when the driven magnetic island width (which is initially zero) exceeds the linear layer width. There are two possible scenarios. Either the system enters its constant-ψ phase prior to the transition to nonlinearity, or *vice versa*. In the former case, we expect the sequence of reconnection regimes to be the inertial regime, followed by the visco-resistive regime, followed by the Ru-

therford regime. In the latter case, we expect the sequence to be the inertial regime, followed by the modified Sweet–Parker regime, followed by the Rutherford regime.

We can distinguish between the two scenarios outlined above by calculating the island width at the (presumed) entry into the linear constant-ψ regime. If this island width is much less than the linear layer width, then the system does indeed enter the linear constant-ψ regime, and there is no Sweet–Parker phase. On the other hand, if the island width is much greater than the linear layer width, then the linear constant-ψ phase is replaced by a Sweet–Parker phase. Now, the system enters the linear constant-ψ regime when $t\sim\tau_2$, at which point the reconnected flux is given by

$$\psi_0\simeq\psi_{\rm VR}(\tau_2)\simeq\frac{E_{sw}\Xi_0\tau_2}{\tau_{\rm VR}}, \tag{51}$$

since $\tau_{\rm on}\ll\tau_2\ll\tau_{\rm VR}$. The associated island width takes the form $W_0=4\sqrt{\psi_0/s}$. Our criterion for the existence of a Sweet–Parker phase is simply $W>\delta_{\rm VR}$ [see Eq. (43)], which yields

$$\Xi_0\gtrsim\frac{s(\mu\eta)^{1/6}}{E_{sw}(sk)^{1/3}}. \tag{52}$$

It follows that the existence of a Sweet–Parker phase is facilitated by a large amplitude wall perturbation and small values of the plasma viscosity and resistivity. The above expression can be rearranged to give

$$\xi_s\gtrsim\delta_{\rm VR}. \tag{53}$$

In other words, a Sweet–Parker phase only occurs when the externally driven plasma displacement at the magnetic resonance exceeds the constant-ψ linear layer width. Equivalently, Eqs. (50) and (53) imply that a Sweet–Parker phase only occurs when the current density in the reconnecting region exceeds the equilibrium current density: i.e.,

$$J\gtrsim J_0. \tag{54}$$

The latter criterion for the onset of Sweet–Parker reconnection is consistent with that proposed by Waelbroeck.[19]

G. Discussion

Our ''inertial'' regime corresponds to regimes *A* and *B* of Hahm and Kulsrud[1] (there is, in fact, no meaningful distinction between the latter two regimes). Note that the inertial regime is unaffected by viscosity. Our ''visco-resistive'' regime corresponds to regime *D* of Hahm and Kulsrud (modified by strong plasma viscosity). Our ''Rutherford'' regime corresponds to phase *E* of Hahm and Kulsrud (see Sec. I). Our ''modified Sweet–Parker'' regime corresponds to regime *W* of Wang and Bhattacharjee[2] (modified by strong plasma viscosity). Note that regime *C* of Hahm and Kulsrud corresponds to the time interval $\tau_1\ll t\ll\tau_2$ during which we can obtain no simple analytic expression for the reconnection rate.

IV. NUMERICAL RESULTS

A. Introduction

Equations (6)–(9), plus the initial equilibrium (10)–(14) and the boundary conditions (15)–(18), have been implemented numerically in a finite-difference code which is second-order in space and first-order in time. The code makes use of the well-known semi-implicit algorithm of Harned and Schnack[20] in order to circumvent the highly restrictive Courant–Freidrichs–Lewy condition on the Alfvén wave. The computational grid is uniform in the y-direction. However, in order to help resolve the reconnecting region, the grid points in the x-direction are more closely packed in the vicinity of the magnetic resonance.

All of the simulations discussed in this paper employ a uniform time-step of 0.01 normalized time units, as well as a 256×128 computational grid. The simulations are performed using a common plasma equilibrium characterized by $X_w=1.5$, $L=3.0$, $E_{ss}=-3.024$, $E_{sw}=0.3431$, $s=0.8193$, and $k=2.094$.

B. Code diagnostics

In the vicinity of the magnetic resonance ($x=0$), Ohm's law (8) is written as

$$\frac{\partial\psi}{\partial t}+\mathbf{V}\cdot\nabla\psi=-\eta j+E_0, \tag{55}$$

where $j\equiv-\nabla^2\psi$ is the current density in the z-direction. Now, by definition, $\nabla\psi=0$ at the magnetic O- and X-points. Since there is zero equilibrium plasma flow, and the boundary perturbation is nonpropagating, the positions of the O- and X-points are fixed and easily identifiable in our simulations. Our reconnected flux diagnostic is defined as

$$\psi_0(t)=\tfrac{1}{2}[\,\psi(\text{X-point})-\psi(\text{O-point})\,], \tag{56}$$

where the factor 1/2 is for consistency with our previous definition of the reconnected flux: i.e., $\psi_0(t)=\psi^{(1)}(0,t)$. Our reconnection rate diagnostic is defined as

$$J(t)=\tfrac{1}{2}[\,j(\text{O-point})-j(\text{X-point})\,]. \tag{57}$$

It follows from Eq. (55), and the fact that $\nabla\psi=0$ at the O- and X-points, that $J=\eta^{-1}\,d\psi_0/dt$. Thus, J measures both the reconnection rate and the current density in the reconnecting region.

C. Inertial regime

Figure 1 illustrates the typical magnetic reconnection seen in our simulations at small times. No reconnection is observed until about 2 Alfvén times after the imposition of the boundary perturbation. This delay (which is not taken into account in the analytic theory) is ascribed to the finite time needed for information to be carried by Alfvén waves from the plasma boundary to the resonant surface. Thereafter, until $t\rightarrow\tau_1$, the reconnection rate matches almost exactly with that predicted theoretically in the inertial regime [see Eq. (35)].

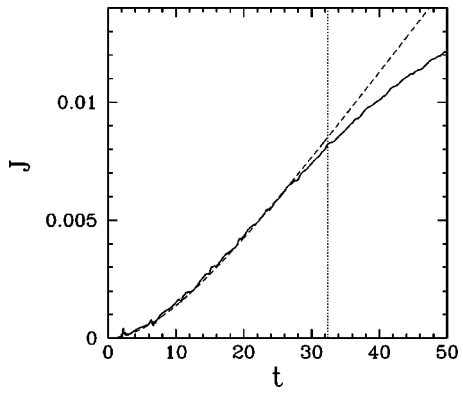

FIG. 1. The reconnection rate, $J(t)$ (solid curve) versus time for a simulation with $X_w=1.5$, $L=3.0$, $\eta=1\times10^{-6}$, $\mu=1\times10^{-5}$, $\Xi_0=1\times10^{-3}$, and $\tau_{on}=10$. The vertical dotted line indicates when $t=\tau_1$. The dashed curve shows the theoretical reconnection rate in the inertial regime, $J_I(t)$.

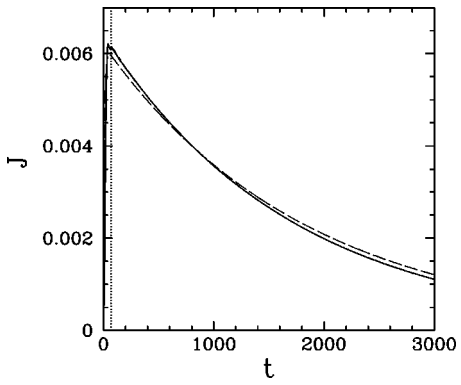

FIG. 3. The reconnection rate, $J(t)$ (solid curve) versus time for a simulation with $X_w=1.5$, $L=3.0$, $\eta=1\times10^{-5}$, $\mu=1\times10^{-4}$, $\Xi_0=1\times10^{-3}$, and $\tau_{on}=10$. The vertical dotted vertical line indicates when $t=\tau_2$. The dashed curve shows the theoretical reconnection rate in the visco-resistive regime, $J_{VR}(t)$.

D. Visco-resistive regime

Figure 2 illustrates the typical magnetic reconnection seen in our simulations at intermediate times. As predicted theoretically, the reconnection rate conforms closely to the inertial rate [see Eq. (35)] when $t<\tau_1$, and to the visco-resistive rate [see Eq. (41)] when $t>\tau_2$. The period $\tau_1<t<\tau_2$, during which we have been unable to obtain a simple analytic expression for the reconnection rate, is characterized by a fairly uneventful switchover from inertial to visco-resistive reconnection.

Figures 3 and 4 illustrate the typical magnetic reconnection seen in our simulations at large times, in cases where the perturbation amplitude is sufficiently small to preclude eventual entry into the nonlinear regime. In such cases, once the system enters the visco-resistive regime it remains in that regime until full reconnection is achieved. Note the close agreement between the theoretical ψ_0 and J values [see Eqs. (40) and (41)] and those obtained from the simulation. Observe that the current J in the reconnecting region builds up in the nonconstant-ψ phase ($t<\tau_2$), reaches a maximum at $t\sim\tau_2$, and then decays exponentially in the constant-ψ phase ($t>\tau_2$) on a typical tearing time-scale, τ_{VR}.

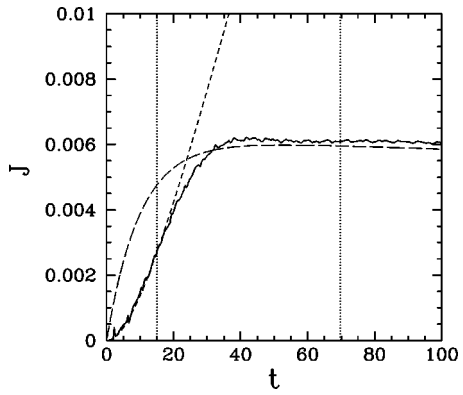

FIG. 2. The reconnection rate, $J(t)$ (solid curve) versus time for a simulation with $X_w=1.5$, $L=3.0$, $\eta=1\times10^{-5}$, $\mu=1\times10^{-4}$, $\Xi_0=1\times10^{-3}$, and $\tau_{on}=10$. The leftmost vertical dotted line indicates when $t=\tau_1$, whereas the rightmost line shows when $t=\tau_2$. The short-dashed curve shows the theoretical reconnection rate in the inertial regime, $J_I(t)$. The long-dashed curve shows the theoretical reconnection rate in the visco-resistive regime, $J_{VR}(t)$.

E. Rutherford regime

Figures 5 and 6 illustrate the typical magnetic reconnection seen in our simulations at large times, in cases where the perturbation amplitude is sufficiently large to allow eventual entry into the nonlinear regime, but not large enough to trigger Sweet–Parker reconnection. It can be seen that after the system enters the constant-ψ regime (at $t=\tau_2$), there is a brief visco-resistive phase (ending at $t\sim400$), followed by a long Rutherford phase (which persists until full reconnection is achieved). Note the close agreement between the theoretical ψ_0 and J values [see Eqs. (45) and (46)] and those obtained from the simulation. Observe that the current J in the reconnecting region builds up in the nonconstant-ψ phase ($t<\tau_2$), reaches a maximum at $t\sim\tau_2$, and then decays algebraically in the constant-ψ phase ($t>\tau_2$) on a typical resistive time-scale, τ_{RF}.

Figure 7 shows a plot of the typical current density pattern around the magnetic island in the Rutherford regime. The island flux surfaces (light) and the magnetic separatrix

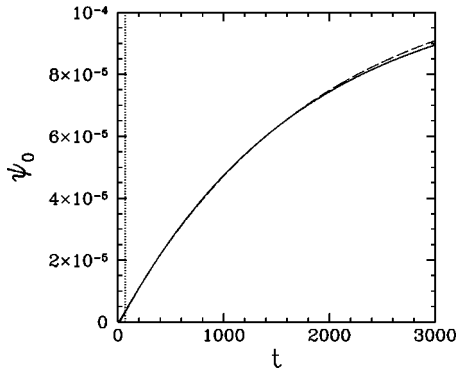

FIG. 4. The reconnected flux, $\psi_0(t)$ (solid curve) versus time for a simulation with $X_w=1.5$, $L=3.0$, $\eta=1\times10^{-5}$, $\mu=1\times10^{-4}$, $\Xi_0=1\times10^{-3}$, and $\tau_{on}=10$. The vertical dotted vertical line indicates when $t=\tau_2$. The dashed curve shows the theoretical reconnected flux in the visco-resistive regime, $\psi_{VR}(t)$.

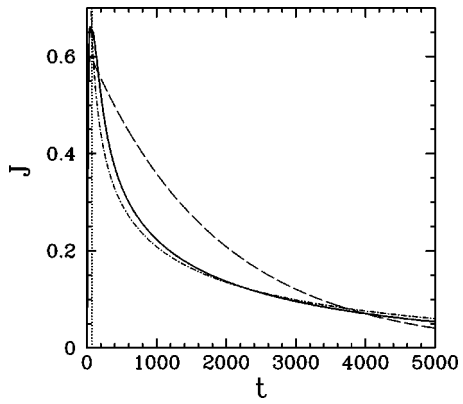

FIG. 5. The reconnection rate, $J(t)$ (solid curve) versus time for a simulation with $X_w=1.5$, $L=3.0$, $\eta=1\times10^{-5}$, $\mu=1\times10^{-4}$, $\Xi_0=1\times10^{-1}$, and $\tau_{\rm on}=10$. The vertical dotted vertical line indicates when $t=\tau_2$. The dashed curve shows the theoretical reconnection rate in the visco-resistive regime, $J_{\rm VR}(t)$. The dot–dashed curve shows the theoretical reconnection rate in the Rutherford regime, $J_{\rm RF}(t)$.

(dark) can be clearly seen. As expected, the reconnecting region (darkest) is strongly localized around the magnetic X-point.

F. Modified Sweet–Parker regime

So far, in all of the cases we have discussed, the analysis of Hahm and Kulsrud (modified to include strong plasma viscosity) offers a complete and highly accurate description of the reconnection dynamics. Figure 8 shows a simulation in which the analysis of Hahm and Kulsrud breaks down, as predicted by Wang and Bhattacharjee, due to the formation of a Sweet–Parker current sheet (see Fig. 11). Note that, unlike all of the previous simulations we have analyzed, the maximum value of the reconnection rate J lies well above the peak visco-resistive value.

G. Onset of Sweet–Parker reconnection

As we have seen, in the absence of a Sweet–Parker phase, the reconnection rate J achieves its maximum value at

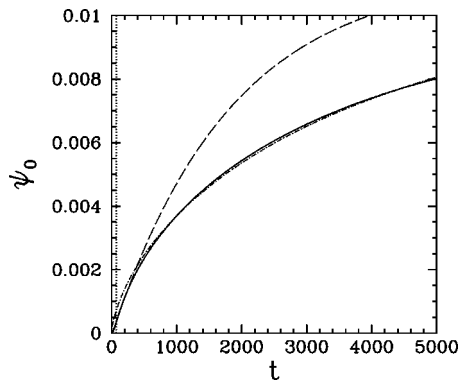

FIG. 6. The reconnected flux, $\psi_0(t)$ (solid curve) versus time for a simulation with $X_w=1.5$, $L=3.0$, $\eta=1\times10^{-5}$, $\mu=1\times10^{-4}$, $\Xi_0=1\times10^{-1}$, and $\tau_{\rm on}=10$. The vertical dotted vertical line indicates when $t=\tau_2$. The dashed curve shows the theoretical reconnected flux in the visco-resistive regime, $\psi_{\rm VR}(t)$. The dot–dashed curve shows the theoretical reconnected flux in the Rutherford regime, $\psi_{\rm RF}(t)$.

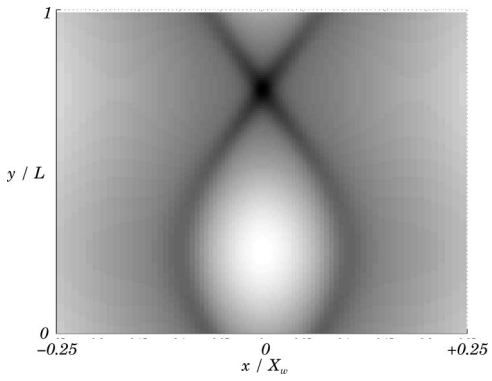

FIG. 7. A plot of the current density, $j(x,y)$, at $t=1000$ for the simulation shown in Figs. 5 and 6. Dark areas correspond to more positive j values and *vice versa*. The magnetic O-point is located at $(0,\ 0.25\,L)$, whereas the X-point is located at $(0,\ 0.75\,L)$.

$t\sim\tau_2$, as the system enters the visco-resistive regime. This observation yields the following prediction for the maximum reconnection rate in the absence of a Sweet–Parker phase [see Eq. (41)]:

$$J_{\max\,\rm VR}=J_{\rm VR}(\tau_2)\simeq\frac{E_{sw}(sk)^{1/3}}{\mathcal{A}(\eta\mu)^{1/6}}\,\Xi_0. \tag{58}$$

Here, we have made use of the ordering $\tau_{\rm on}\ll\tau_2\ll\tau_{\rm VR}$. Note that $J_{\max\,\rm VR}$ scales *linearly* with the perturbation amplitude Ξ_0. As we have also seen, in the presence of a Sweet–Parker phase, the maximum reconnection rate lies well above $J_{\max\,\rm VR}$. Moreover, as is apparent from Eq. (49), $J_{\max}$ scales as $\Xi_0^{3/2}$ in this case. Thus, it should be possible to detect the onset of Sweet–Parker reconnection by monitoring the ratio $J_{\max}/\Xi_0$: i.e., the maximum reconnection rate over the perturbation amplitude. In the absence of a Sweet–Parker phase, this ratio should take the value $E_{sw}(sk)^{1/3}/[\mathcal{A}(\eta\mu)^{1/6}]$, which is independent of Ξ_0. On the other hand, in the presence of a Sweet–Parker phase, the ratio should rise above the value $E_{sw}(sk)^{1/3}/[\mathcal{A}(\eta\mu)^{1/6}]$, and increase with increasing Ξ_0, approximately as $\Xi_0^{1/2}$.

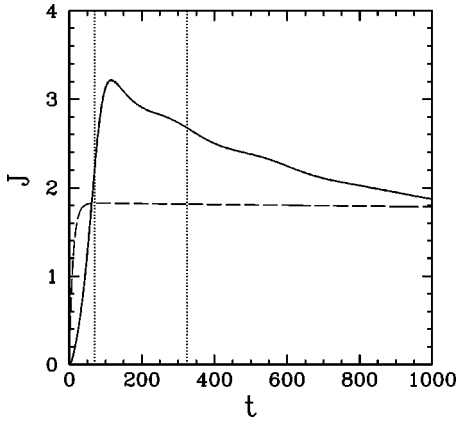

FIG. 8. The reconnection rate, $J(t)$ (solid curve) versus time for a simulation with $X_w=1.5$, $L=3.0$, $\eta=1\times10^{-7}$, $\mu=1\times10^{-6}$, $\Xi_0=6.4\times10^{-2}$, and $\tau_{\rm on}=10$. The leftmost vertical dotted line indicates when $t=\tau_1$, whereas the rightmost line shows when $t=\tau_2$. The dashed curve shows the theoretical reconnection rate in the visco-resistive regime, $J_{\rm VR}(t)$.

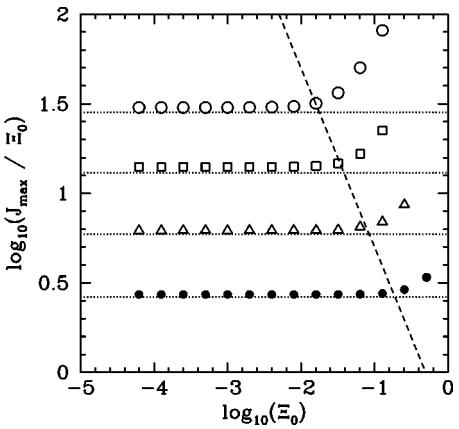

FIG. 9. The maximum reconnection rate, $J_{\max}$, divided by the perturbation amplitude, Ξ_0, plotted versus the perturbation amplitude. All simulations have $X_w=1.5$, $L=3.0$, and $\tau_{\rm on}=10$. The open circles show simulations with $\eta=1\times10^{-7}$ and $\mu=1\times10^{-6}$. The open squares show simulations with $\eta=1\times10^{-6}$ and $\mu=1\times10^{-5}$. The open triangles show simulations with $\eta=1\times10^{-5}$ and $\mu=1\times10^{-4}$. The solid circles show simulations with $\eta=1\times10^{-4}$ and $\mu=1\times10^{-3}$. The dotted horizontal lines show the corresponding theoretical $J_{\max}/\Xi_0$ values in the absence of a Sweet–Parker reconnection phase [see Eq. (58)]. The dashed diagonal line corresponds to $J_{\max}=0.5$.

Figure 9 shows the maximum reconnection rate divided by the perturbation amplitude, as a function of the perturbation amplitude, for a series of simulations with widely differing η and μ values. At low perturbation amplitudes, and fixed η and μ, the ratio $J_{\max}/\Xi_0$ takes the constant value predicted by Eq. (58). However, above a critical perturbation amplitude, the ratio rises above the value predicted by Eq. (58), and starts to increase with increasing Ξ_0—thus, indicating the onset of Sweet–Parker reconnection. The analysis of Sec. III F suggests that the onset of Sweet–Parker reconnection should correspond to $J_{\max}\gtrsim J_c$ [see Eq. (54)], where J_c is an $O(1)$ constant. The diagonal line shown in Fig. 9 is the locus of $J_{\max}=0.5$. It can be seen that this line corresponds fairly accurately to the onset of Sweet–Parker reconnection. Thus, we conclude that the expressions for the critical perturbation amplitude given in Sec. III F are essentially correct.

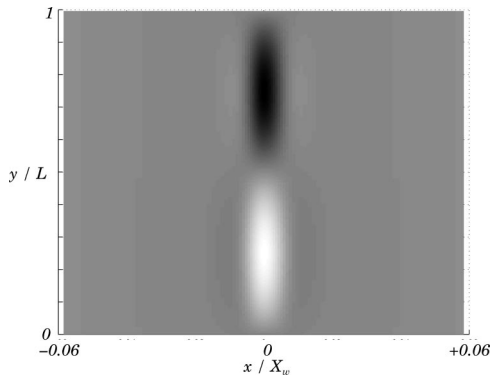

FIG. 10. A plot of the current density, $j(x,y)$, at $t=300$ for a simulation with $\eta=1\times10^{-7}$, $\mu=1\times10^{-6}$, $\Xi_0=4\times10^{-3}$, and $\tau_{\rm on}=10$. Dark areas correspond to more positive j values and *vice versa*. The magnetic O-point is located at (0, 0.25 L), whereas the X-point is located at (0, 0.75 L).

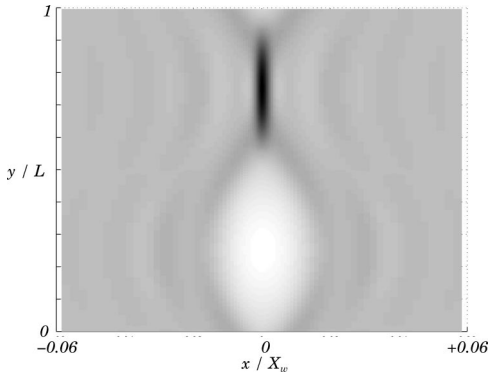

FIG. 11. A plot of the current density, $j(x,y)$, at $t=200$ for a simulation with $\eta=1\times10^{-7}$, $\mu=1\times10^{-6}$, $\Xi_0=6.4\times10^{-2}$, and $\tau_{\rm on}=10$. Dark areas correspond to more positive j values and *vice versa*. The magnetic O-point is located at (0, 0.25 L), whereas the X-point is located at (0, 0.75 L).

In order to check that our interpretation of Fig. 9 is reasonable, Figs. 10 and 11 show the current patterns (close to the peak reconnection rate) in the vicinity of the magnetic resonance for typical data-points in Fig. 9 lying to the left and to the right of the diagonal line, respectively. Figure 10, which corresponds to the maximum reconnection rate in the absence of a Sweet–Parker phase, quite clearly shows (as expected) the current pattern characteristic of a *linear* reconnection regime, with symmetric regions of positive and negative current perturbation. On the other hand, Fig. 11, which corresponds to the maximum reconnection rate in the presence of a Sweet–Parker phase, quite clearly shows the current pattern characteristic of Sweet–Parker reconnection, with an intense extended current sheet centered on the magnetic X-point. Note, from Fig. 7, that the characteristic current patterns in the constant-ψ Rutherford and nonconstant-ψ Sweet–Parker regimes are easily distinguishable.

V. SUMMARY AND CONCLUSIONS

We have employed two-dimensional MHD simulations to investigate the so-called Taylor problem, in which a small amplitude boundary perturbation is suddenly applied to a tearing stable, slab plasma equilibrium—the perturbation being such as to drive magnetic reconnection within the plasma. Incidentally, this type of reconnection, which is not due to an intrinsic plasma instability, is generally known as ''forced reconnection.'' For numerical reasons the investigation is restricted to the large magnetic Prandtl number limit, $\mu/\eta\gg1$. Our simulation results are highly consistent with the analysis of Hahm and Kulsrud[1] (modified by strong plasma viscosity).

In all cases, we find that the initial reconnection conforms closely to that predicted theoretically in the so-called inertial regime, which is discussed in Sec. III C. In the limit in which the perturbation switch-on time, $\tau_{\rm on}$, approaches zero, the reconnected flux is predicted to increase initially like $\psi_0\sim\eta t^2$: i.e., on the classical Sweet–Parker reconnection time-scale, $\eta^{-1/2}$. It should be noted, however, that reconnection in the inertial regime is quite different from Sweet–Parker reconnection, and any resemblance of the characteristic time-scales is purely coincidental.

As predicted by Wang and Bhattacharjee,[2] we find that the analysis of Hahm and Kulsrud breaks down at large perturbation amplitudes, due to the formation of a Sweet–Parker current sheet. We have derived an expression for the critical perturbation amplitude required to trigger Sweet–Parker reconnection (see Sec. III F), and have successfully benchmarked it against numerical simulations. When applied to forced reconnection in tokamak plasmas, our criterion for Sweet–Parker reconnection takes the approximate form

$$\frac{b_\theta}{B_\theta} \gtrsim \frac{P^{1/6}}{S^{1/3}}, \tag{59}$$

where b_θ is the typical poloidal field change associated with the external perturbation, B_θ the typical equilibrium poloidal field-strength, S the Lundquist number of the plasma (i.e., $1/\eta$), and P the Prandtl number (i.e., μ/η). Very roughly speaking, tokamak plasmas are characterized by $P \sim 10$ and $S \lesssim 10^8$ (the larger the tokamak, the hotter the plasma, and the larger the S value). Moreover, typical values of b_θ/B_θ lie in the range 10^{-4} to 10^{-2}. For small amplitude perturbations characterized by $b_\theta/B_\theta \simeq 10^{-4}$ (e.g., error-fields), we find that Sweet–Parker reconnection is triggered when $S \gtrsim 10^{12}$. We conclude that such perturbations could never drive Sweet–Parker reconnection in tokamak plasmas, no matter how rapid their onset. For large amplitude perturbations characterized by $b_\theta/B_\theta \simeq 10^{-2}$ (e.g., very large MHD instabilities), we find that Sweet–Parker reconnection is triggered when $S \gtrsim 10^6$. We conclude that such perturbations could possibly drive Sweet–Parker reconnection, but only in large tokamaks.

ACKNOWLEDGMENTS

The author gratefully acknowledges helpful discussions with A. Bhattacharjee, X. Wang, and A. Ishizawa during the preparation of this paper.

This research was funded by the U.S. Department of Energy under Contract No. DE-FG05-96ER-54346 as well as via Cooperative Agreement No. DE-FC02-01ER54652 under the auspices of the program for Scientific Discovery through Advanced Computing.

[1] T. S. Hahm and R. M. Kulsrud, Phys. Fluids **28**, 2412 (1985).
[2] X. Wang and A. Bhattacharjee, Phys. Fluids B **4**, 1795 (1992).
[3] Z. W. Ma, X. Wang, and A. Bhattacharjee, Phys. Plasmas **3**, 2427 (1996).
[4] J. Rem and T. J. Schep, Plasma Phys. Controlled Fusion **40**, 139 (1998).
[5] G. Veckstein and R. Jain, Phys. Plasmas **5**, 1506 (1998).
[6] G. Veckstein and R. Jain, Phys. Plasmas **6**, 2897 (1999).
[7] A. Ishizawa and S. Tokuda, Phys. Plasmas **7**, 875 (2000).
[8] A. Bhattacharjee, R. Fitzpatrick, and X. Wang, Phys. Plasmas **8**, 374 (2001).
[9] A. Ishizawa and S. Tokuda, Phys. Plasmas **8**, 376 (2001).
[10] J. T. Scoville, R. J. La Haye, A. G. Kellman, T. H. Osborne, R. D. Stambaugh, E. J. Strait, and T. S. Taylor, Nucl. Fusion **31**, 875 (1991).
[11] G. M. Fishpool and P. S. Haynes, Nucl. Fusion **34**, 109 (1994).
[12] C. C. Hegna, J. D. Callen, and R. J. La Haye, Phys. Plasmas **6**, 130 (1999).
[13] P. H. Rutherford, Phys. Fluids **16**, 1903 (1973).
[14] P. A. Sweet, *Electromagnetic Phenomena in Cosmical Physics* (Cambridge University Press, New York, 1958).
[15] E. N. Parker, J. Geophys. Res. **62**, 509 (1957).
[16] H. P. Furth, J. Killeen, and M. N. Rosenbluth, Phys. Fluids **6**, 459 (1963).
[17] R. Fitzpatrick, Phys. Plasmas **1**, 3308 (1994).
[18] W. Park, D. A. Monticello, and R. B. White, Phys. Fluids **27**, 137 (1984).
[19] F. L. Waelbroeck, Phys. Rev. Lett. **70**, 3259 (1993).
[20] D. S. Harned and D. D. Schnack, J. Comput. Phys. **65**, 57 (1986).